Geophys. J. Int. (2013) **195,** 192–199
Advance Access publication 2013 August 7
doi: 10.1093/gji/ggt262

Domain-wall dynamics in 4C pyrrhotite at low temperature

J. Kind,[1,5] I. García-Rubio,[2] M. Charilaou,[3] N. R. Nowaczyk,[4] J. F. Löffler[5] and A. U. Gehring[1]

[1] *Institute of Geophysics, ETH Zurich,* 8092 *Zurich, Switzerland. E-mail: jessica.kind@erdw.ethz.ch*
[2] *Laboratory of Physical Chemistry, ETH Zurich,* 8093 *Zurich, Switzerland*
[3] *Department of Physics, University of California, Berkeley, CA* 94720-7300, *USA*
[4] *Helmholtz Centre Potsdam, GFZ German Research Centre for Geosciences,* 14473 *Potsdam, Germany*
[5] *Laboratory of Metal Physics and Technology, Department of Materials, ETH Zurich,* 8093 *Zurich, Switzerland*

Accepted 2013 July 3. Received 2013 July 3; in original form 2013 February 18

SUMMARY

Monoclinic 4C pyrrhotite (Fe_7S_8) is ferrimagnetic due to an ordered defect structure with alternating vacancy and vacancy-free sublattices. Its low-temperature magnetic transition near 35 K is characterized by the distinct increase in coercivity and remanent magnetization. The increase of these parameters has been attributed to changes in the domain wall structure. We present static and dynamic magnetization data of a powder sample to study the domain-wall dynamics across the low-temperature transition. The amplitude-dependent ac susceptibility and the ferromagnetic resonance spectroscopy indicate that the hardening of the domain-wall pinning at the transition occurs simultaneously with the decrease in initial saturation remanent magnetization. These two effects are explained by the enhanced inhomogeneity of the bulk material caused by the persistency of the ordered vacancies and by newly formed defects due to localized distortion of Fe(II) sites in the vacancy-free sublattice. The generated localized defects are the link between the domain wall dynamics and the low-temperature transition in 4C pyrrhotite.

Key words: Magnetic mineralogy and petrology; Rock and mineral magnetism; Defects.

1 INTRODUCTION

Pyrrhotite ($Fe_{1-x}S$) refers to a non-stoichiometric iron sulphide with a compositional range x varying between 0.08 and 0.125. Pyrrhotite has attracted increasing interest in rock and palaeomagnetism, because this monosulphide is an important remanence carrier in the Earth's crust where it commonly occurs as accessory mineral in metamorphic and pegmatitic rock bodies and as a major constituent in sulphide ore deposits (Hall 1986; Rickard & Luther 2007). Moreover, pyrrhotite is also known from extraterrestrial materials such as chondrites and interplanetary dust particles (e.g. Bradley 1988; Zolensky & Thomas 1995; Rochette *et al.* 2001). The magnetic properties have been used to detect pyrrhotite in geological systems (Fillion & Rochette 1988; Rochette *et al.* 1990) and as a proxy to infer pressure-induced processes in the crust, probably caused by shock waves related to impacts (Vaughan & Tossell 1973; Kontny *et al.* 2000; Gattacceca *et al.* 2007; Louzada *et al.* 2010; Gilder *et al.* 2011).

The investigation of natural pyrrhotite has revealed a variety of chemical compositions with hexagonal structure and antiferromagnetic ordering or monoclinic structure and ferrimagnetic ordering (Arnold 1967; Pearce *et al.* 2006). The stoichiometric monosulphide troilite (FeS) crystallizes in a hexagonal structure that bases upon the NiAs structure (e.g. Bertaut 1953; Carpenter & Desborough 1964; Hafner & Kalvius 1966; Wang & Salveson 2005). With departure from stoichiometry by removing di-valent Fe cations from octahedral sites, the layer stacking remains hexagonal with respect to the S atoms and the vacancy-bearing layers determine the structural and magnetic properties of the pyrrhotite. In Fe_7S_8, a predominant mono-sulphide in geological systems, the omission of Fe(II) leads to a superstructure, in which vacancies are arranged in alternating layers along the c-axis with those free of vacancies (Bertaut 1953; Li *et al.* 1996; Powell *et al.* 2004). The dimension of this supercell along the c-axis is four times that of the NiAs structure with a small distortion of the interaxial angle that lowers the symmetry from hexagonal to monoclinic (Tokonami *et al.* 1972; Powell *et al.* 2004). Thus Fe_7S_8 is denoted as monoclinic 4C pyrrhotite.

The 4C pyrrhotite with stacked layers of Fe(II) and S ions shows strong ferrimagnetic behaviour below the Curie temperature of about 600 K that originates from uncompensated moments between alternating vacancy and vacancy-free layers. The cations have ferromagnetic coupling within the layers and antiferromagnetic coupling between adjacent layers (Néel 1953). Monoclinic pyrrhotite reveals an intrinsic low-temperature transition at about 35 K, which can be magnetically detected by a distinct demagnetization and by the drastic increase in the hysteresis parameters B_c and M_r upon cooling (Fillion & Rochette 1988; Dekkers 1989; Rochette *et al.* 1990). At

room temperature the magnetization of the 4C pyrrhotite exhibits a strong uniaxial anisotropy with the easy magnetization direction in the (001) basal plane and the hard axis of magnetization along the crystallographic *c*-axis (Weiss 1907; Bin & Pauthenet 1963; Sato *et al.* 1964). The pronounced uniaxiality critically affects the domain structure. Studies using the Bitter pattern technique revealed wide domains separated by 180° walls (Soffel 1981; Halgedahl & Fuller 1983; O'Reilly *et al.* 2000). Halgedahl & Fuller (1983) studied the domain-walls in applied fields and they showed two different cases, particles with fully developed, reversible walls and particles that are partially controlled by the absence of nucleation, which prohibits the generation of discernible domain-wall patterns, probably due to strong energy traps near the grain surface. This is considered as a metastable single-domain state at remanence (Halgedahl & Fuller 1983). Dekkers (1989) reported a grain-size dependent increase of the characteristic coercivity of the hysteresis associated with the low-temperature transition that they interpreted as domain effect, that is, a conversion of a multidomain state into a pseudo-single-domain or single-domain state below the transition. Given the above, the question arises of the relation between intrinsic low-temperature transition and domain-wall dynamics, which is of interest when taking this transition as characteristic for the identification of 4C pyrrhotite particles in terrestrial and extraterrestrial systems. In this study, we exploit the static and dynamic magnetic response of multidomain 4C pyrrhotite in order to evaluate its domain-wall properties at low temperature.

2 SAMPLE AND METHODS

In this study, we used a pyrrhotite specimen from the Dalnegorsk ore field in Russia, where a large variety of sulphide minerals formed during skarn-type mineralization. A powder sample was produced from a centimetre-sized single crystal by crushing and grinding in an agate mortar. The composition of the pyrrhotite was magnetically inferred from the Curie temperature using a multifunction kappabridge with an applied field of 300 A m^{-1} and a frequency of 875 Hz (MKF-1). The static magnetic properties of the pyrrhotite between 300 and 10 K were analysed by magnetization and remanence experiments. The temperature behaviour of the saturation isothermal remanent magnetization (SIRM) acquired in a 1.5 T field at 300 K, termed as initial SIRM, was measured down to 10 K. In addition, the SIRM measurements followed the zero-field cooled (ZFC)/field cooled (FC) protocol by Moskowitz *et al.* (1993), where the sample is first cooled in a zero field to 10 K followed by acquiring a magnetization in a 2.5 T field and then warming to room temperature in the absence of a field. The same procedure was repeated while the 2.5 T field was applied during cooling. Magnetization curves were obtained in fields of up to 1.5 T at selected temperatures and the hysteresis parameters, including saturation magnetization (M_s), saturation remanence (M_r) and coercivity (B_c) were recorded. It is worth noting that M_s is a pseudo-saturation, because the powder sample is not fully saturated in the 1.5 T field. To avoid effects of the magnetic history on the hysteresis parameters, prior to every hysteresis loop the sample was warmed up to room temperature and a remanence was acquired using a 1.5 T field. In addition, the hysteresis loops at 10 K were recorded after FC in a 1.5 T field. All experiments were performed using a Quantum Design Physical Property Measurement System (PPMS) with a 9 T superconducting magnet.

The dynamic magnetic properties of the sample were determined by frequency as well as amplitude dependence of the low-field ac susceptibility (amplitude 0.1–1.5 mT, frequency 10–10 000 Hz) and ferromagnetic resonance (FMR) spectroscopy in the temperature range as above. The amplitude dependence of the in- and the out-of-phase (χ', χ'') susceptibilities were analysed on the same sample as used in the static measurements using the PPMS with a resolution of 1 K between 10 and 300 K and in high resolution of 0.1 K between 15 and 50 K.

The dynamic magnetic analyses were complemented by FMR experiments. In FMR spectroscopy, the precessional motion (Larmor precession) of the magnetization in an external magnetic field is sustained by a microwave magnetic field, perpendicular to the external field (e.g. Kittel 1948; Vonsovskii 1966). In a field-sweep experiment, resonance occurs when the Larmor precession frequency equals the microwave frequency. The resonance equation can then be written as $\hbar\nu = g_{\rm eff}\mu_B B_{\rm eff}$, where $\hbar$ is the Planck's constant, ν is the microwave frequency, μ_B is the Bohr magneton (9.274×10^{24} Am^2), $g_{\rm eff}$ is the gyromagnetic factor, and $B_{\rm eff}$ is the effective field. This field is the sum of the applied dc magnetic field and the internal field of the sample that contains different contributions such as demagnetization field (shape anisotropy), magnetocrystalline anisotropy field, and magnetostrictive energies. The last contribution can be neglected because pyrrhotite exhibits no remarkable magnetostriction (Dunlop & Özdemir 1997; Powell *et al.* 2004). In a powder sample, the crystallites are oriented randomly and each fulfils a specific resonance condition, such that the measured net signal is the superposition of all resonance events. The effective field $B_{\rm eff}$ at maximum absorption is defined as the resonance field $B_{\rm res}$ and is obtained from the zero-crossing in the derivative spectrum (point of inflection). The corresponding splitting factor defined as $g_{\rm eff}$ can be extracted using the above resonance equation. For the FMR measurements the powder sample was fixed with paraffin in a standard ESR quartz glass tube with a diameter of 4 mm. The spectra were recorded using a Bruker E500 spectrometer working at the X-band (microwave frequency of 9.47 GHz) in a dc field between 5 and 700 mT. The temperature of the sample in the cavity was controlled by means of a helium gas-flow cryostat ESR 910 (Oxford Instruments), which allowed performing measurements between 10 and 300 K. A modulation amplitude of 1 mT and a microwave power of 0.063 mW were used for the measurements. The low-temperature series was obtained after cooling the sample in the spectrometer cavity to 10 K while the magnet was switched off, measuring the spectrum, and then subsequent recording of the spectra at higher temperatures. In addition spectra were recorded at 10 K in a ZFC/FC experiment that included cooling the sample in the cavity in the absence of a magnetic field, followed by warming up the sample to 300 K and cooling again to 10 K in a 700 mT field.

3 RESULTS AND DISCUSSION

Fig. 1 shows the high-temperature susceptibility measurements of the powder sample. The warming curve exhibits an increase above 500 K, followed by a drop at 596 K, which is considered to be the Curie temperature (T_c) of 4C pyrrhotite (Haraldsen 1941; Schwarz & Vaughan 1972). The increase prior to T_c is probably due to structural reorganization of the vacancies (e.g. Li *et al.* 1996). The decay of the magnetization at T_c is caused by long-range disorder of vacancies associated with the structural change. This link between structural change and magnetic ordering was shown experimentally by neutron diffraction (Powell *et al.* 2004). The well-defined T_c suggests that our powder sample consists of 4C pyrrhotite, and other non-stoichiometric iron sulphides can be neglected. The difference

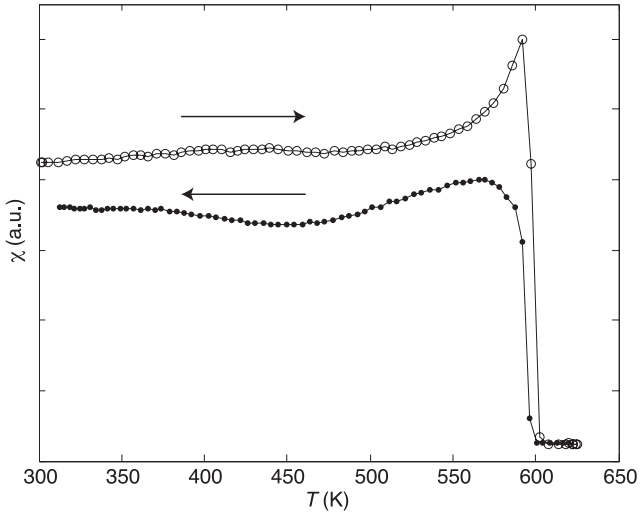

Figure 1. Magnetic susceptibility upon heating and cooling with the Curie temperature at 596 K.

between the heating and cooling curves of our 4C pyrrhotite reveals a loss of magnetization when cooling the sample from $T > T_c$. This loss can be explained by relatively slow diffusion that impedes the formation of alternating vacancy and vacancy-free layers during fast cooling through the T_c (Bennett & Graham 1981).

3.1 Static magnetic properties

The initial SIRM cooling curve between 300 and 10 K shows a maximum at about 150 K and a pronounced drop of about 20 per cent between 40 and 25 K (Fig. 2a). The ZFC-FC SIRM warming curves between 10 and 300 K are similar and show a remanence decay of about 90 per cent up to 36 K (Fig. 2b). At higher temperatures the decrease is continuous with relative flattening above 150 K. At 300 K, 2 per cent of the acquired remanence is preserved. The kink at 36 K marks the magnetic transition. The ZFC and FC warming curves up to the transition are similar with a nearly linear decay between 10 and 20 K (Fig. 2). The marked low-temperature behaviour is also seen in the magnetic hysteresis parameters. At room temperature $M_s = 21.23$ Am^2 kg^{-1}, $M_r = 1.23$ Am^2 kg^{-1}, and

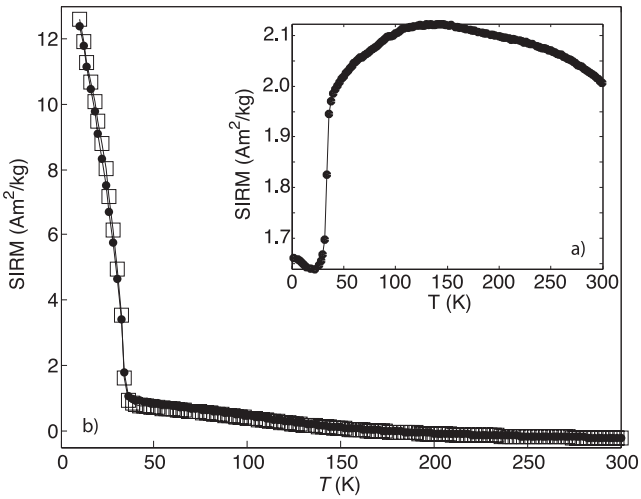

Figure 2. (a) Cooling of the initial saturation isothermal remanent magnetization (SIRM) and (b) the SIRM warming curves after ZFC (squares) and FC (circles).

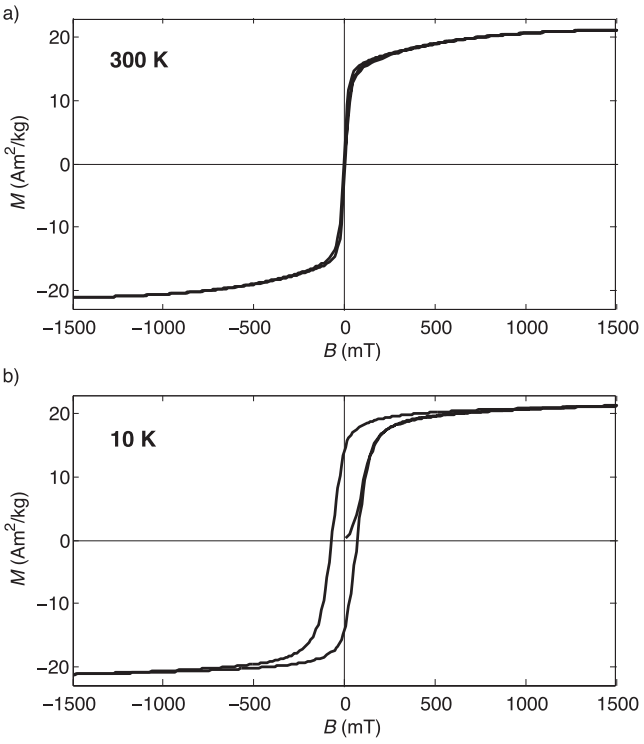

Figure 3. Hysteresis loops at (a) 300 K and (b) 10 K.

the coercivity $B_c = 3.2$ mT (Fig. 3a). The saturation magnetization remains nearly constant over the whole temperature range. Similar values were reported for pyrrhotite from different geological sites (Dekkers 1988). It is worth noting that the magnetic moment in the powder sample is not fully saturated in a 1.5 T field (Fig. 3). This is in agreement with experimental and theoretical results that showed the hard magnetization along the [001] axes has a nearly paramagnetic behaviour (Besnus *et al.* 1968; Weiss 1907). Furthermore, the M_r/M_s ratio is 0.06. The hysteresis parameters are indicative of pyrrhotite in a multidomain state. At 10 K after ZFC, the hysteresis parameters are $M_s = 21.32$ Am^2 kg^{-1}, $M_r = 14.47$ Am^2 kg^{-1}, $M_r/M_s = 0.68$ and $B_c = 70.9$ mT (Fig. 3b). The hysteresis parameters after FC in a 1.5 T field exhibit no significant changes. The initial magnetization after FC considered as M_r at 10 K, however, was more than one magnitude higher than after ZFC with the initial magnetization of 0.22 Am^2 kg^{-1}, that is, the inherited M_r acquired at 300 K.

The hysteresis parameters show a drastic change between 10 and 36 K. Upon heating to 20 K, the B_c halves, M_r and M_r/M_s decrease to 11.40 Am^2 kg^{-1} and 0.53, respectively (Table 1). This change coincides with the linear decay of the SIRM upon heating (Fig. 2b). At higher temperatures the hysteresis parameters further decrease and at 36 K, $B_c = 7.8$ mT and $M_r/M_s = 0.13$. Up to 150 K a slight decrease is found, and between 150 and 300 K the hysteresis parameters are stable as also indicated by the nearly linear behaviour of the ZFC/FC SIRM curves (Fig. 2; Table 1). Furthermore, the temperature dependence of B_c accompanied with the transition can be described by an exponential fit $B_c(T) = B_0 \exp(\alpha T)$ with $B_0 = 156$ mT and the constant $\alpha = -0.08$ (Fig. 4). The exponential temperature dependence of B_c can be due to domain-wall dynamics (Mukherjee *et al.* 2000), but such behaviour can also originate from intrinsic exchange interactions as reported for hemo-ilmenite solid solutions (Charilaou *et al.* 2011). Because pyrrhotite exhibits no temperature dependence of the pseudo-M_s, the exponential

Table 1. Hysteresis and FMR parameters of the powder sample. At 10 K, the hysteresis and FMR parameters were determined after ZFC (1) and FC (2).

Temp. (K)	B_c (mT)	M_r ($Am^2\ kg^{-1}$)	M_s ($Am^2\ kg^{-1}$)	B_{res} (mT)	g_{eff}
10 (1)	70.9	14.47	21.32	200.8	3.51
10 (2)	70.9	14.47	21.40	200.8	3.51
20	34.6	11.40	21.49	206.4	3.42
25	20.9	9.39	22.46		
30	11.6	6.10	22.37	211.8	3.33
33	9.3	3.86	21.49	214.2	3.29
36	7.8	2.64	21.05	215.9	3.27
38				218.2	3.23
40	7.5	3.33	20.79	218.9	3.22
50	5.5	2.81	21.58	227.2	3.10
70				236.7	2.98
90				241.7	2.92
120				246.8	2.86
150	3.3	2.19	21.58	251.0	2.81
180				254.5	2.77
210				258.5	2.73
230				260.8	2.70
300	3.2	1.23	21.23	267.8	2.63

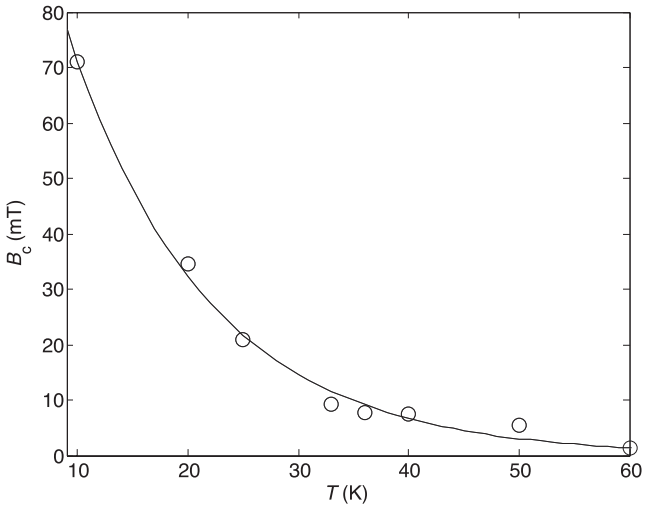

Figure 4. Temperature dependence of B_c at temperatures between 10 and 50 K and its exponential fitting function $B_c(T) = B_0 \exp(\alpha T)$ with $B_0 = 156$ mT and $\alpha = -0.08$.

increase of B_c is attributed to the domain-wall dynamics. Considering the static measurements it can be summarized that the pyrrhotite powder sample shows a well-defined transition at 36 K and at lower temperature the magnetic hardness of the samples is mainly affected by the domain-wall dynamics.

3.2 Dynamic magnetic properties

The ac susceptibility exhibits below 36 K a drop followed by a weak peak in the χ' that is associated with a peak and a shoulder in the χ'' (Figs 5a and b). The in-phase component has no frequency dependence, whereas the out-of-phase component shows a weak dependence down to 36 K (Fig. 5a). In contrast, an amplitude dependence was found for both, the in-phase and the out-of-phase component above 25 K (Fig. 5b). This dependence suggests reversible domain-wall oscillation in the pyrrhotite grains (Worm *et al.* 1993; Jackson *et al.* 1998). The field dispersion of χ' and χ'' is nearly constant down to about 36 K, where the low-temperature transition of the 4C pyrrhotite is indicated by the drop of χ' and a cusp in χ'' (Fig. 5b). At lower temperature the field dispersion narrows, and vanishes at 25 K. This suggests that the domains are smeared out upon freezing or their walls are strongly pinned, so that the total interaction energy of the domain-walls with the lattice defect is significantly increased.

In the following, FMR spectral properties are used to obtain further insight into the domain properties of the pyrrhotite sample. At 300 K, the X-band FMR spectrum exhibits $B_{res} = 267.8$ mT, corresponding to $g_{eff} = 2.63$, and the peak-to-peak line-width $\Delta B = 231$ mT (Fig. 6). Rotation of the sample tube in the cavity shows nearly no spectral change as it is expected for powder samples. The few published X-band FMR spectra of monoclinic pyrrhotite exhibited non-unique absorption properties (e.g. Mikhlin *et al.* 2002; Chang *et al.* 2012). Fujimura & Torizuka (1956) reported a FMR spectrum of a pyrrhotite single crystal along the easy axis of magnetization in the (001) plane with a very broad line-width that was assigned to magnetic interactions of microcrystals within the sample. It has to be mentioned that in X-band FMR spectra the pyrrhotite bulk material is not saturated because of the large uniaxial anisotropy with easy magnetization direction in the (001) plane and a hard magnetization direction along the [001] axis (Bin & Pauthenet 1963). Therefore, to obtain meaningful X-band FMR spectra, perfect single crystals with well-defined anisotropy axes or powder samples with randomly distributed anisotropy axes should be used. In the latter case, anisotropy properties cannot be extracted quantitatively, but semiquantitative information about structural properties, such as domain-walls and impurities/point-defects of the bulk sample, can be inferred.

In FMR experiments on multidomain particles, the low-field absorption is affected by domain-wall motions (Rado *et al.* 1950; Gehring *et al.* 2009). Bitter patterns of pyrrhotite at room temperature revealed that domain-walls are generally moved out of the grains in fields of up to about 200 mT (Halgedahl & Fuller 1983). Considering domain-wall motions in applied fields, it can be assumed that B_{res} of 231 mT at 300 K arises from grains in a single-domain-like state. In such a state the demagnetization field of a grain is enhanced compared to the remanence state, where the grain is a multidomain. The demagnetization field is opposite to the external field and, therefore, the stronger the demagnetization field, the higher the B_{res} and the lower the g_{eff}. The FMR spectra obtained from our pyrrhotite sample are nearly identical after repeated recording at 300 K. This suggests a domain-wall dynamics with reversible nucleation upon removal of the magnetic field. In contrast, the FMR spectra recorded at 10 K are different after ZFC and FC in a 700 mT field (Fig. 6). In the ZFC case the spectral recording starts from a nearly demagnetized state, whereas FC generates a relatively strong remanence magnetization. Both spectra have $B_{res} = 200.8$ mT and nearly identical high-field absorptions, $B > B_{res}$ (Fig. 6; Table 1). In the low-field range ($B < B_{res}$) the ZFC sample exhibits an increasing absorption with an inflection point at about 70 mT, whereas the sample after FC exhibits a concave-shaped absorption (Fig. 6). The different low-field behaviour can be explained by the change of the domain structure after applying a field of 0.7 T. In the newly formed domain structure more spins are aligned to the external field and these spins fulfill the resonance conditions at lower fields. Mastrogiacomo *et al.* (2010) described such remanence effect in FMR spectra obtained from magnetite chains. For the pyrrhotite sample the remanence effect is compensated at $B = 170$ mT, where the ZFC/FC FMR spectra merge (Fig. 6). Given this, the shape of the FMR absorption in the low-field range of the ZFC sample is used as a measure of the different pinning energies

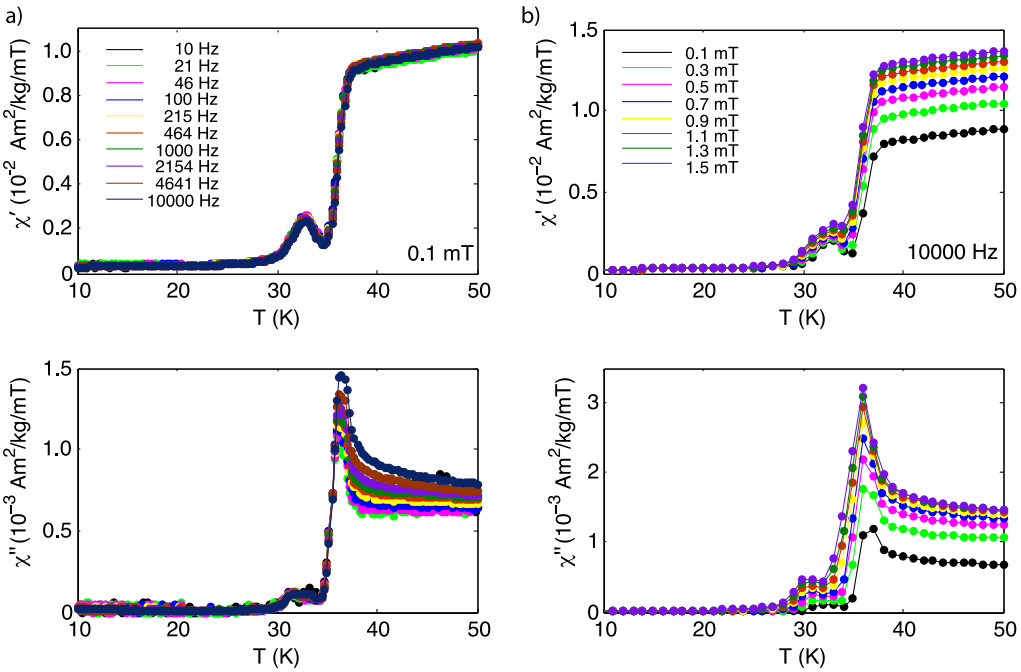

Figure 5. (a) Frequency and (b) amplitude dependence of the in-phase (χ') and out-of-phase (χ'') ac magnetic susceptibility as a function of temperature.

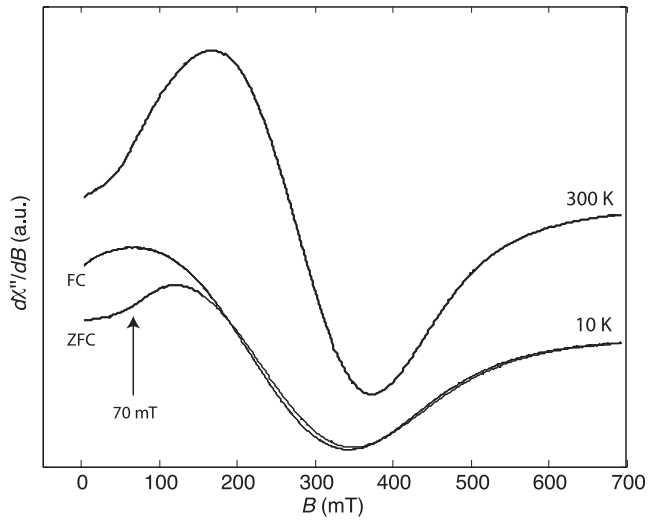

Figure 6. Ferromagnetic resonance spectra recorded at 300 K and 10 K after ZFC and FC. The inflection point in the low-field range is marked by an arrow.

of domain-walls, and that in turn has been considered as the microcoercivity of a sample (Xu & Merrill 1990). The inflection point at about 70 mT can then be taken as average microcoercivity (Fig. 6). Xu & Merrill (1990) showed for a magnetite that the average microcoercivity is equal to B_c of the bulk material with relatively hard-pinned 180° domain-walls. This correlation is in accordance with the low-field FMR data and $B_c = 70.9$ mT obtained from our sample at 10 K (Fig. 6; Table 1).

Fig. 7 shows the low-temperature FMR series between 10 and 300 K. Upon warming the FMR spectra slightly narrow and B_{res} shifts to higher values. The shift of B_{res} with temperature can be schematically subdivided into two ranges. Between 90 and 300 K, B_{res} increases nearly linearly. Below 70 K a pronounced change of B_{res} is indicated by the maximum slope at 38 K (Fig. 8). Changes of B_{res} are generally caused by magnetocrystalline and/or shape anisotropy (demagnetization field). Comparing the shift of B_{res} with the temperature-dependent magnetocrystalline anisotropy constants K_3 and K_4 (Bin & Pauthenet 1963), no clear correlation is evident. Therefore, it is feasible to postulate that the change of B_{res} is critically affected by the demagnetization field. In multidomain particles demagnetization is determined by the domain structure. Domains reduce the demagnetization field and in turn the internal field in powder samples. This can explain the shift of B_{res} between 10 and 300 K. The strongest demagnetization field at 300 K is because at $B_{res} = 267.8$ mT the grains are in a single-domain-like state. Domain-walls that remained pinned in the grains can then cause the decrease of B_{res}. Below 70 K this effect becomes more pronounced and the highest increase of strongly pinned domain-walls in the grains occurs at 38 K, close to the low-temperature transition. At 10 K, B_{res} is reduced by about 25 per cent that points to marked departure from the metastable single-domain state at 300 K.

4 DOMAIN-WALL DYNAMICS AND LOW TEMPERATURE TRANSITION

The low-temperature magnetic transition in our monoclinic pyrrhotite at 36 K is characterized by the decrease of the initial SIRM and by marked changes of the hysteresis parameters. A similar behaviour of the magnetic properties was reported previously (Fillion & Rochette 1988; Dekkers *et al.* 1989; Rochette *et al.* 1990). Considering the hysteresis parameters, the increase in B_c and M_r associated with the magnetic transition is similar to that observed for the classical Verwey transition in magnetite (Verwey 1939; Özdemir & Dunlop 1999). Therefore, it was postulated that the transition in pyrrhotite is of Verwey-like type with a structural change and a subsequent marked increase of the magnetocrystalline anisotropy (Fillion & Rochette 1988). Wolfers *et al.* (2011) proposed that the magnetic transition corresponds to a structural change from monoclinic at room temperature to triclinic at low temperature. This contradicts the neutron diffraction results by Powell *et al.* (2004) that showed no change of the crystallographic structure at low

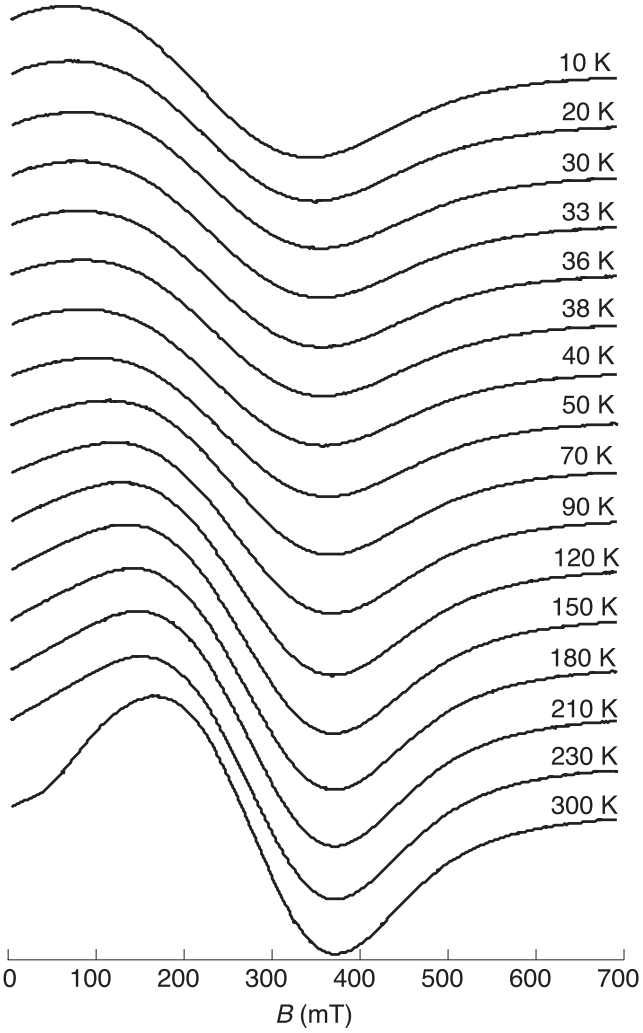

Figure 7. The evolution of the ferromagnetic resonance spectra between 10 and 300 K.

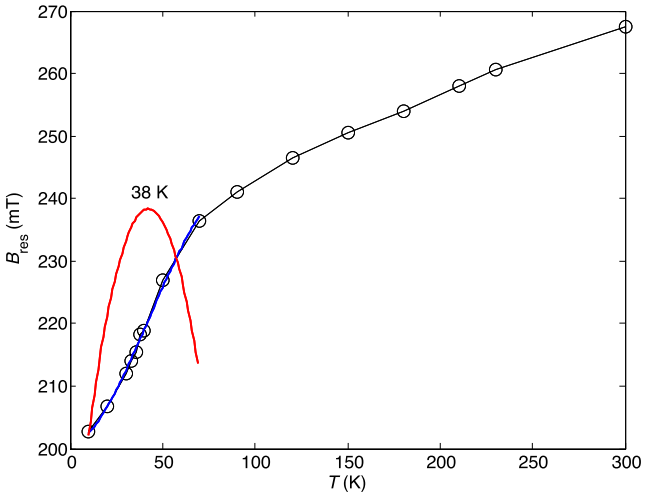

Figure 8. Resonance field B_{res} as a function of temperature. The maximum slope at 38 K in the low temperature range was determined by the first derivative (red) of the fitted (blue) curve.

temperature and by the low temperature behaviour of the magnetocrystalline anisotropy constants K_3 and K_4 (Bin & Pauthenet 1963). Evidence for the absence of a crystallographic change at the low-temperature transition can be deduced by comparing the ZFC/FC SIRM data of pyrrhotite with those of magnetite. The latter exhibits below the Verwey transition a different behaviour of the ZFC and FC SIRM curve (e.g. Moskowitz *et al.* 1993; Özdemir & Dunlop 1999; Fischer *et al.* 2008). This difference is due to the structural change from cubic to monoclinic and the shift of the magnetic easy axes from [111] to [001] associated with the Verwey transition (Muxworthy & McClelland 2000; Wright *et al.* 2002). In contrast the nearly identical ZFC and FC SIRM curves for our monoclinic pyrrhotite indicates no detectable symmetry change below the transition (Fig. 2b). Moreover, no frequency dependence in the ac susceptibility is observed below the transition (Fig. 5a). This behaviour is not in accordance with that of the Verwey transition and suggests different physical mechanisms in 4C pyrrhotite and magnetite at low temperature (e.g. Fischer *et al.* 2008; Özdemir *et al.* 2009). Furthermore, the absence of structural change at the transition is supported by B_{res} of the FMR spectra at 10 K. For pyrrhotite, B_{res} is identical for the ZFC and FC case, whereas for magnetite, B_{res} of the FC spectrum is shifted towards lower field compared to the ZFC spectrum (Gehring *et al.* 2011). Because the magnetocrystalline anisotropy field contributes to B_{res}, identical values for pyrrhotite also argue against a change of the crystallographic structure.

Neutron diffraction data of a powder sample by Powell *et al.* (2004) provided direct evidence that the magnetization easy axes in 4C pyrrhotite are in the (001) plane at 300 K and they are rotated by 29° towards the [001] axis at 11 K. Bin & Pauthenet (1963) calculated the rotation out of the (001) basal plane, using the magnetocrystalline anisotropy constants K_3 and K_4 according to $\theta_0 = \arccos(-K_3/2K_4)^{1/2}$. They found an overall rotation of about 18°, which is significantly lower than the value obtained from neutron diffraction (Powell *et al.* 2004). Using the above equation, however, the rotation starts at about 205 K and decreases linearly down to about 40 K. At lower temperatures, the rotation is less than 1°. This behaviour suggests that the low-temperature demagnetization in 4C pyrrhotite is not directly affected by the spin rotation out of the (001) plane as known for the Morin transition in hematite (Morin 1950; de Boer *et al.* 2001). Considering the above line of argumentation the domain wall dynamics at the low-temperature transition is neither controlled by a change of the crystallographic lattice nor by spin rotation. Moreover, the simultaneous occurrence of the decreasing initial SIRM upon cooling and changes in the domain wall dynamics suggest a link between the two phenomena.

Gilder *et al.* (2011) reported decreasing SIRM of multidomain 4C pyrrhotite under high pressure. Mössbauer data indicate that the effect of pressure on the magnetic properties is due to the high-spin to low-spin spin crossover of Fe(II) in octrahedral sites (Vaughan & Tossell 1973; Takele & Hearne 2001). In our sample, the behaviour of M_s at low temperature argues against a spin crossover in the Fe(II) sites of the vacancy and vacancy-free layers. Mössbauer spectroscopy under ambient pressure provides evidence for changes in the ligand fields of the Fe(II) sites in the vacancy-free layers below the transition (Oddou *et al.* 1992). This has been explained by invoking a Jahn-Teller effect. Considering the structure of 4C pyrrhotite, this effect is likely localized in the vicinity of the vacancies. Such localized effect would enhance the structural inhomogeneity and probably cause the drop of the initial SIRM at the transition. With this in mind, the cusp in χ'' can then be attributed to the dissipation due to localized structural changes in the vacancy-free layers (Figs 5a and b). The amplitude dependence of χ'' shows that the domain wall dynamics are affected by the transition. The cease of the field dispersion at 25 K indicates the loss of domain-wall oscillation,

that is, hardening of the pinned domain-walls. This magnetic hardening below the transition agrees well with the exponential temperature dependence of B_c, because the coercivity field is related to the total interaction energy of 180° domain-walls with lattice defects (Kronmüller & Fähnle 2003). Given this, the localized structural changes generate defects that enhance the domain-wall pinning.

5 CONCLUSION

The domain-wall dynamics in 4C pyrrhotite is associated with the low-temperature transition. The loss of the domain-wall reversibility and the subsequent hardening of domain-wall pinning below the transition are explained by the enhanced structural inhomogeneity of the material. This enhancement originates from the persistence of the lattice defects in the vacancy layers and from distorted Fe(II) sites formed in the vacancy-free layers at low temperature. The simultaneous occurrence of the decreasing initial SIRM and the cease of the domain wall dynamics are both critically affected by the localized structural changes in the vacancy-free layers of 4C pyrrhotite.

ACKNOWLEDGEMENTS

The authors like to thank M. Jackson and an anonymous reviewer for the critical comments that were helpful to improve the manuscript. This research was supported by the Swiss National Science Foundation Grant No. 200021-121844 and PBEZP2-142894 (MC).

REFERENCES

Arnold, R.G., 1967. Range in composition and structure of 82 natural terrestrial pyrrhotites, *Can. Mineral.,* **9,** 31–50.

Bennett, C.E.G. & Graham, J., 1981. New observations on natural pyrrhotites. magnetic transition in hexagonal pyrrhotite, *Am. Mineral.,* **66,** 1254–1257.

Bertaut, E.F., 1953. Contribution a l'étude des structures lacunaires: la pyrrhotine, *Acta Crystallogr.,* **6,** 557–561.

Besnus, M.J., Munschy, G. & Meyer, A.J.P., 1968. Sublattice rotation in ferrimagnets: the case of pyrrhotite, *J. appl. Phys.,* **39,** 903–904.

Bin, M. & Pauthenet, R., 1963. Magnetic anisotropy in pyrrhotite, *J. appl. Phys.,* **34,** 1161–1162.

de Boer, C.B., Mullender, T.A. & Dekkers, M.J., 2001. Low-temperature behaviour of haematite: susceptibility and magnetization increase on cycling through the Morin transition, *Geophys. J. Int.,* **146,** 201–216.

Bradley, J.P., 1988. Analysis of chondritic interplanetary dust thin-sections, *Geochim. Cosmochim. Acta,* **52,** 889–900.

Carpenter, R.H. & Desborough, G.A., 1964. Range in solid solution and structure of naturally occurring troilite and pyrrhotite, *Am. Mineral.,* **49,** 1350–1365.

Chang, L., Winklhofer, M., Roberts, A.P., Dekkers, M.J., Horng, C.-S., Hu, L. & Chen, Q., 2012. Ferromagnetic resonance characterization of greigite (Fe_3S_4), monoclinic pyrrhotite (Fe_7S_8), and non-interacting titanomagnetite ($Fe_{3-x}Ti_xO_4$), *Geochem. Geophy. Geosy.,* **13**(Q05Z41), 1–19.

Charilaou, M., Löffler, J.F. & Gehring, A.U., 2011. Slow dynamics and field-induced transitions in a mixed-valence oxide solid solution, *Phys. Rev. B,* **83,** 224414_1–22441_7.

Dekkers, M.J., 1988. Magnetic properties of natural pyrrhotite Part I: Behaviour of initial susceptibility and saturation-magnetization-related rock-magnetic parameters in a grain-size dependent framework, *Phys. Earth planet. Inter.,* **53,** 376–393.

Dekkers, M.J., 1989. Magnetic properties of natural pyrrhotite. II. High- and low-temperature behaviour of J_{rs} and TRM as function of grain size, *Phys. Earth planet. Inter.,* **57,** 266–283.

Dekkers, M.J., Mattéi, J.-L., Fillion, G. & Rochette, P., 1989. Grain-size dependence of the magnetic behavior of pyrrhotite during its low-temperature transition at 34 K, *Geophys. Res. Lett.,* **16,** 855–858.

Dunlop, D. & Özdemir, Ö., 1997. *Fundamental Frontiers,* Cambridge University Press.

Fillion, G. & Rochette, P., 1988. The low temperature transition in monoclinic pyrrhotite, *J. Phys.,* **C8,** 907–908.

Fischer, H., Mastrogiacomo, G., Löffler, J.F., Warthmann, R.J., Weidler, P.G. & Gehring, A.U., 2008. Ferromagnetic resonance and magnetic characteristics of intact magnetosome chains in *Magnetospirillum gryphiswaldense*, *Earth planet. Sci. Lett.,* **270,** 200–208.

Fujimura, T. & Torizuka, Y., 1956. Ferromagnetic resonance absorption in a pyrrhotite single crystal, *J. Phys. Soc. Jap.,* **11,** 327–327.

Gattacceca, J., Rochette, P., Boustie, M. & Berthe, L., 2007. The effects of explosive-driven shocks on the natural remanent magnetization and the magnetic properties of rocks, *Phys. Earth planet. In.,* **162,** 85–98.

Gehring, A.U., Fischer, H., Louvel, M., Kunze, K. & Weidler, P.G., 2009. High temperature stability of natural maghemite: A magnetic and spectroscopic study, *Geophys. J. Int.,* **179,** 1361–1371.

Gehring, A.U., Fischer, H., Charilaou, M. & García-Rubio, I., 2011. Magnetic anisotropy and Verwey transition of magnetosome chains in *Magnetospirillum gryphiswaldense*, *Geophys. J. Int.,* **187,** 1215–1221.

Gilder, S.A., Egli, R., Hochleitner, R., Roud, S.C., Volk, M.W.R., Le Goff, M. & de Wit, M., 2011. Anatomy of a pressure-induced, ferrimagnetic to paramagnetic transition in pyrrhotite: implications for the formation pressure of diamonds, *J. geophys. Res.,* **116,** B10101, doi:10.1029/2011JB008292.

Hafner, S. & Kalvius, M., 1966. The Mössbauer resonance of Fe^{57} in troilite (FeS) and pyrrhotite ($Fe_{0.88}S$), *Z. Kristallogr.,* **123,** 443–458.

Halgedahl, S. & Fuller, M., 1983. The dependence of magnetic domain structure upon magnetization state with emphasis upon nucleation as a mechanism for pseudo-single domain behavior, *J. geophys. Res.,* **88,** 6505–6522.

Hall, A.J., 1986. Pyrite-pyrrhotine redox reactions in nature, *Mineral. Mag.,* **50,** 223–229.

Haraldsen, H., 1941. Über die eisen (II) sulfid Mischkristalle, *Z. anorg. Chem.,* **246,** 169–194.

Jackson, M., Moskowitz, B., Rosenbaum, J. & Kissel, C., 1998. Field-dependence of ac susceptibility in titanomagnetites, *Earth planet. Sci. Lett.,* **157**(3-4), 129–139.

Kittel, C., 1948. On the theory of ferromagnetic resonance absorption, *Phys. Rev.,* **73,** 155–161.

Kontny, A., de Wall, H., Sharp, T.G. & Pósfai, M., 2000. Mineralogy and magnetic behavior of pyrrhotite from a 260 degrees C section at the KTB drilling site, Germany, *Am. Mineral.,* **85,** 1416–1427.

Kronmüller, H. & Fähnle, M., 2003. *Micromagnetism and the Microstructure of Ferromagnetic Solids,* Cambridge University Press.

Li, F., Franzen, H.F. & Kramer, M.J., 1996. Ordering, incommensuration, and phase transitions in pyrrhotite. Part I: a TEM study of Fe_7S_8, *J. Solid State Chem.,* **124,** 264–271.

Louzada, K.L., Stewart, S.T., Weiss, B.P., Gattacceca, J. & Bezaeva, N.S., 2010. Shock and static pressure demagnetization of pyrrhotite and implications for the martian crust, *Earth planet. Sci. Lett.,* **290**(1/2), 90–101.

Mastrogiacomo, G., Fischer, H., García-Rubio, I. & Gehring, A.U., 2010. Ferromagnetic resonance spectroscopic response of magnetite chains in a biological matrix, *J. Magn. Magn. Mater.,* **322,** 661–663.

Mikhlin, Yu.L., Kuklinskiy, A.V., Pavlenko, N.I., Varnek, V.A., Asanov, I.P., Okotrub, A.V., Selyutin, G.E. & Solovyev, L.A., 2002. Spectroscopic and XRD studies of the air degradation of acid-reacted pyrrhotites, *Geochim. Cosmochim. Acta,* **66**(23), 4057–4067.

Morin, F.J., 1950. Magnetic susceptibility of α-Fe_2O_3 and α-Fe_2O_3 with added titanium, *Phys. Rev.,* **78,** 819–820.

Moskowitz, B.M., Frankel, R.B. & Bazylinski, D.A., 1993. Rock magnetic criteria for the detection of biogenic magnetite, *Earth planet. Sci. Lett.,* **120,** 283–300.

Mukherjee, S., Ranganathan, R. & Mondal, P., 2000. Field cooled coercivity in $La_{1-x}Sr_xCoO_3$, *J. Phys. Chem. Solids,* **61,** 1433–1438.

Muxworthy, A.R. & McClelland, E., 2000. Review of the low-temperature magnetic properties of magnetite from a rock magnetic perspective, *Geophys. J. Int.,* **140,** 101–114.

Néel, L., 1953. Some new results on antiferromagnetism & ferromagnetism, *Rev. Mod. Phys.,* **25,** 58–63.

Oddou, J.L., Jeandey, C.H., Mattei, J.L. & Fillion, G., 1992. Mössbauer study of the low-temperature transition in pyrrhotite, *J. Magn. Magn. Mater.,* **104,** 1987–1988.

O'Reilly, W., Hoffmann, V., Chouker, A.C., Soffel, H.C. & Menyeh, A., 2000. Magnetic properties of synthetic analogues of pyrrhotite ore in the grain size range 1-24μm, *Geophys. J. Int.,* **142,** 669–683.

Özdemir, Ö. & Dunlop, D.J., 1999. Low-temperature properties of a single crystal of magnetite oriented along principal magnetic axes, *Earth planet. Sci. Lett.,* **165**(2), 229–239.

Özdemir, Ö., Dunlop, D.J. & Jackson, M., 2009. Frequency and field dependent susceptibility of magnetite at low temperature, *Earth Planets Space,* **61,** 125–131.

Pearce, C.I., Pattrick, R.A.D. & Vaughan, D.J., 2006. Electric and magnetic properties of sulfides, *Rev. Min. Geochem.,* **61,** 127–180.

Powell, A.V., Vaqueiro, P., Knight, K.S., Chapon, L.C. & Sánchez, R.D., 2004. Structure and magnetism in synthetic pyrrhotite Fe_7S_8: a powder neutron-diffraction study, *Phys. Rev. B,* **70,** 014415, doi:10.1103/PhysRevB.70.014415.

Rado, G.T., Wright, R.W. & Emerson, W.H., 1950. Ferromagnetism at very high frequencies. III. Two mechanisms of dispersion in a ferrite, *Phys. Rev.,* **80,** 273–280.

Rickard, D. & Luther, G.W., 2007. Chemistry of iron sulfides, *Chem. Rev.,* **107,** 514–562.

Rochette, P., Fillion, G., Matteí, J.L. & Dekkers, M.J., 1990. Magnetic transition at 30-34 K in Fe_7S_8: insight into a widespread occurence of pyrrhotite in rocks, *Earth planet. Sci. Lett.,* **98,** 319–328.

Rochette, P., Lorand, J.-P., Fillion, G. & Sautter, V., 2001. Pyrrhotite and the remanent magnetization of SNC meteorites: a changing perspective on Martian magnetism, *Earth planet. Sci. Lett.,* **190,** 1–12.

Sato, K., Yamada, M. & Hirone, T., 1964. Megnetocrystalline anisotropy of pyrrhotite, *J. Phys. Soc. Japan,* **19,** 1592–1595.

Schwarz, E.J. & Vaughan, D.J., 1972. Magnetic phase relations of pyrrhotite, *J. Geomagn. Geoelectr.,* **24,** 441–458.

Soffel, H.C., 1981. Domain structure of natural fine-grained pyrrhotite in a rock matrix (diabase), *Phys. Earth planet. Inter.,* **26,** 98–106.

Takele, S. & Hearne, G.R., 2001. Magnetic-electronic pressure studies of natural iron-bearing minerals and materials using 57Fe Mössbauer spectroscopy in a diamond anvil cell, *Nucl. Instruments Methods Phys. Res., B,* **183,** 413–418.

Tokonami, M., Nishiguchi, K. & Morimoto, N., 1972. Crystal structure of a monoclinic pyrrhotite (Fe_7S_8), *Am. Mineral.,* **57,** 1066–1080.

Vaughan, D.J. & Tossell, J.A., 1973. Magnetic transitions observed in sulfide minerals at elevated pressures and their geophysical significance, *Science,* **179,** 375–377.

Verwey, E.J.W., 1939. Electronic conduction of magnetite (Fe_3O_4) and its transition point at low temperatures, *Nature,* **144,** 327–328.

Vonsovskii, S.V., 1966. *Ferromagnetic Resonance: The Phenomenon of Resonant Absorption of a High-Frequency Magnetic Field in Ferromagnetic Substances*. Pergamon Press.

Wang, H. & Salveson, I., 2005. A review on the mineral chemistry of the non-stoichiometric iron sulphide, $Fe_{1-x}S$ (0 x 0.125): polymorphs, phase relations and transitions, electronic and magnetic structures, *Phase Trans.,* **78,** 547–567.

Weiss, P., 1907. L'hypothese du champ moleculaire et la propriete ferromagnetique, *J. Phys.,* **6,** 661–690.

Wolfers, P., Fillion, G., Ouladdiaf, B., Ballou, R. & Rochette, P., 2011. The pyrrhotite 32 K magnetic transition, *Solid State Phenom.,* **170,** 174–179.

Worm, H.-U., Clark, D. & Dekkers, M.J., 1993. Magnetic susceptibility of pyrrhotite: grain size, field and frequency dependence, *Geophys. J. Int.,* **114,** 127–137.

Wright, J.P., Attfield, J.P. & Radaelli, P.G., 2002. Charge ordered structure of magnetite Fe_3O_4 below the Verwey transition, *Phys. Rev. B,* **66,** 214422, doi:10.1103/PhysRevB.66.214422.

Xu, S. & Merrill, R., 1990. Microcoerivity, bulk coercivity and saturation remanence in multidomain materials, *J. geophys. Res.,* **95**(B5), doi:10.1029/89JB03064.

Zolensky, M.E. & Thomas, K.L., 1995. Iron and iron-nickel sulfides in chondritic interplanetary dust particles, *Geochim. Cosmochim. Acta,* **59,** 4707–4712.